

CALCULATIONS FOR STEADY PROPAGATION OF A GENERIC RAM ACCELERATOR CONFIGURATION USING THE ROE METHOD *

Matthew J. Grismer[†] and Joseph M. Powers[‡]

Department of Aerospace and Mechanical Engineering,
University of Notre Dame,
Notre Dame, Indiana 46556-5637.

Abstract

This study describes a methodology and gives analysis to determine the steady propagation speed of a projectile fired into a gaseous mixture of fuel and oxidizer. For tractability, the steady supersonic flow of an inviscid calorically perfect ideal reacting gas with high activation energy over a symmetric double wedge, unconfined by a cowl, is considered. Propagation speeds are found which give rise to shocks of such strength as to induce a reaction zone to be in a region which allows the combustion-induced thrust to balance the wave drag. For a fixed heat release greater than a critical value, two steady propagation speeds are predicted. The solution at the higher Mach number is stable to quasi-static perturbations while the solution at the lower Mach number is unstable. This methodology can be applied to analyze devices which have more complex geometries, such as the ram accelerator or oblique detonation wave engine.

Introduction

It is possible to employ oblique shock waves to induce combustion to generate thrust. Recent discussion has been motivated by the ram accelerator, which has been used to propel projectiles to high speeds, and the oblique detonation wave engine (ODWE), which has been proposed to propel the National Aerospace Plane (NASP). For such devices, it is of fundamental importance to have a theory which can predict a steady propagation speed. The numerical analyses of Brackett and Bogdanoff¹ and Yungster and Bruckner², which consider geometries and material properties similar to potential operating conditions for $H_2 - O_2$ systems, and Rankine-Hugoniot

analyses of Powers and Gonthier³ and Powers et. al.⁴, which considers idealized systems in order to retain tractability, predict such speeds in the approximate range 5,000 – 10,000 m/s.

In this paper we briefly review some of the relevant literature, describe a general methodology for determining the steady propagation speed of either ram accelerator projectiles or ODWE-powered aerospace planes, present a simple model problem used to illustrate the methodology, and finally discuss the results of a numerical analysis. Much of the discussion and analysis was first given in Ref. 3 and 4; the new contribution of the present paper is to verify the trends and results of the earlier work with improved numerical solutions of the model equations. To this end, a new code based on the Roe method⁵ was developed and verified on a number of one- and two-dimensional problems; it provides much improved resolution at discontinuities relative to the results of Ref. 4.

Review

The ram accelerator (see Fig. 1) was first tested by Hertzberg, *et al.*^{6,7}. In this application, a high speed

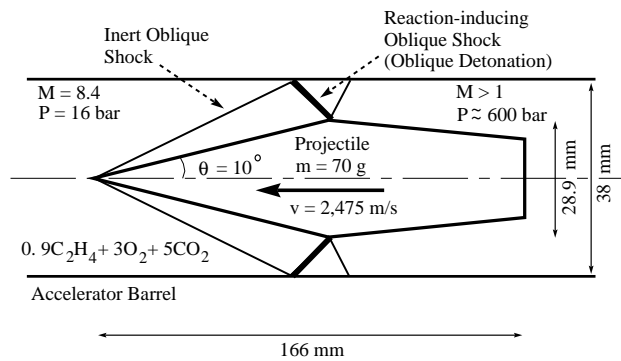


Figure 1: Schematic of ram accelerator, adopted from Hertzberg, *et al.*⁷

projectile is fired at high velocity from a light gas gun

*Copyright © American Institute of Aeronautics and Astronautics, Inc., 1994. All rights reserved.

[†]Graduate Assistant, currently assigned to Wright Laboratory, Wright-Patterson AFB, Ohio, Member AIAA.

[‡]Assistant Professor, Member AIAA.

into a tube filled with an unreacted mixture of combustible gases. Hertzberg, *et al.*⁷ observed that upon entering a 16 m length, 38 mm bore tube filled in its first three stages with varying combinations of CH_4 , O_2 , N_2 , and He at a pressure of 31 bar and in its final stage with $0.9C_2H_4 + 3O_2 + 5CO_2$ at a pressure of 16 bar, that a shock-induced combustion process accelerated a 70 g projectile from an initial velocity of near 1,200 m/s to a velocity of 2,475 m/s (corresponding to a Mach number, $M = 8.4$) at the end of the tube, at which location it was still accelerating. Downstream pressures in the neighborhood of 600 bar were measured. The diameter of the main body of the projectile was 28.9 mm. Its length was 166 mm and the leading edge conical half-angle $\theta = 10^\circ$. Four stabilizing fins (not shown) of diameter 38 mm were a part of the aft-body. A portion of the oblique shock train is sketched in Fig. 1; the various expansion fans and wave interactions are not included. Figure 1 depicts the first reflected shock triggering significant chemical reaction; the temperature-sensitive reaction would be associated with the lead shock for faster projectile speeds, and with a downstream shock for slower speeds. For even slower speeds, the reaction would be downstream of the projectile. It was suggested that such a device can be scaled for direct launch to orbit, for hypervelocity impact studies, and for a hypersonic test facility.

A number of numerical studies of ram accelerators have been performed. Brackett and Bogdanoff¹ used a Godunov scheme to solve the Euler equations combined with one global Arrhenius rate expression for all the chemical reactions. They found that an oblique detonation could occur where the initial conical shock attached to the projectile nose reflected off the tube wall. An oblique detonation could also be induced by placing a small ramp at the midpoint of the projectile body. In either case, they found positive thrust on the projectile, but did not look for steady propagation speeds. Yungster, Eberhardt, and Bruckner⁸ developed a code to solve the Euler equations with detailed multispecies, multireaction chemistry and real gas effects. The code was verified using experimental results for hypersonic, exothermic blunt body flows, and then applied to a ram accelerator configuration at two flight speeds. In the both cases there was a positive thrust on the projectile. Yungster and Bruckner² then performed a detailed study using the code, investigating the performance characteristics of various projectile configurations in the range of 5-10 km/s. They examined the effects of varying projectile geometry, tube cross sectional area, and gas mixture on the net thrust developed on the projectile. They found positive

thrusts in all cases, but did not determine steady propagation speeds. Yungster⁹ studied the shock-wave/boundary-layer interaction on a ram accelerator configuration using a code developed to solve the Reynolds-averaged Navier-Stokes equations with detailed multispecies, multireaction chemistry and a Baldwin-Lomax algebraic turbulence model. The analysis centered on an oblique detonation propulsion mode, and indicated that a reflected shock wave initiated significant combustion in the boundary layer on the projectile. If the projectile speed was increased, significant combustion began in the boundary layer spontaneously. For one flight speed the thrust on the projectile was determined, and it was found to be approximately 10 percent lower than the corresponding inviscid case.

Another relevant propulsion device is the proposed oblique detonation wave engine (ODWE). The idea of using an ODWE for supersonic combustion for a high-speed plane has existed for decades (*e.g.* Dunlap, *et al.*¹⁰). The hypothesized operation is as follows (see Fig. 2). Supersonic air enters the inlet. On-board fuel

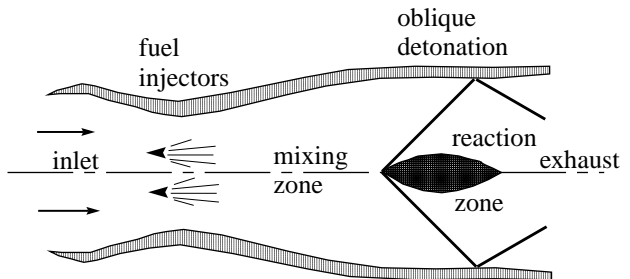


Figure 2: Envisioned oblique detonation wave engine, adopted from Dunlap, *et al.*¹⁰

is injected downstream which mixes with the air without significant reaction. The mixture then encounters a downstream wedge. The oblique shock associated with the wedge compresses and ignites the mixture, generating a propulsive force. Relative to conventional air-breathing engines with subsonic combustion, Dunlap, *et al.* cite the ODWE's advantages as 1) simpler supersonic inlet diffuser design since the inherently supersonic oblique detonation does not require deceleration to a subsonic state, 2) reduced total pressure losses, 3) shorter combustion chamber length, 4) no ignition device other than the wedge, and 5) faster flight velocities. Cited concerns are 1) the lack of static thrust, 2) uncertainty as to whether mixing lengths are practical, and 3) uncertainty with regards to the process's stability.

Methodology and Model Problem

Most recent theoretical studies related to ram accelerators and ODWE's⁸⁻²⁰ have not given analysis to determine a steady propagation speed. Typically these studies treat the related problem of flow with a fixed incoming Mach number over a fixed geometry and concentrate on discussing the features of the resulting flow field. Only a small number of incoming Mach numbers are studied. The problems posed are physical in the sense that one could envision an experiment in which the projectile is fixed in a wind tunnel in which the incoming Mach number is controllable. Such an approach, however, yields little about what the steady speed of a freely propagating vehicle should be.

Here we present a general theoretical approach to predict the steady speed. One first selects a mathematical model for the fluid and a representative geometry. The model equations are studied in the reference frame in which the projectile is stationary; thus, the incoming flow velocity, which is the steady propagation speed, is thought of as an adjustable parameter at this stage. For a given incoming velocity, solution of the model equations leads to a stress distribution on the projectile surface which may or may not result in a net force on the projectile. Should the particular incoming velocity lead to zero net force on the projectile, that velocity is a candidate for a steady propagation speed. The static stability of the candidate solutions is easily determined. Should a perturbation in the incoming velocity lead to a net force which tends to restore the projectile to its speed at which there is zero net force, the solution is stable in a static sense (we call such solutions stable); otherwise the solution is unstable. A further step, not considered here, is to account for the inertia of the projectile and surrounding fluid so as to determine the dynamic stability.

This methodology is illustrated through the use of a model problem which is related to the ram accelerator and ODWE. For tractability, we consider an idealized model and geometry which retain the essential physics of the real devices. The geometry, shown in Fig. 3, is a symmetric double wedge with half angle θ and length \tilde{L} . Two cowl surfaces are placed symmetrically about the wedge and are separated by height \tilde{H} . The depth of the double wedge and cowl is taken to be infinite and the flow is assumed to have no variation in this direction. The Cartesian coordinate system, with its origin at the leading edge and with the \tilde{x} axis aligned with the incoming flow is also indicated. It is appropriate to think of a ram accelerator as the axisymmetric analog of Fig. 3 in which the projectile moves while the cowl is stationary; likewise, an aerospace plane powered by an ODWE can

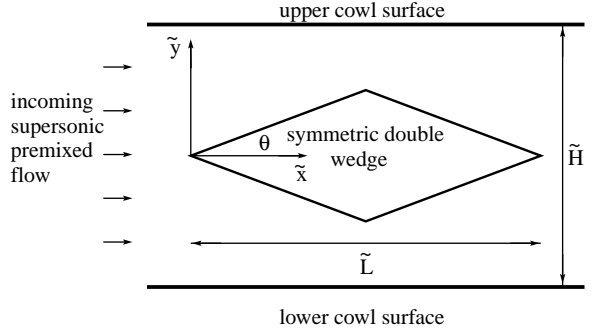


Figure 3: Schematic of generic configuration

be thought of as the axisymmetric analog of Fig. 3 in which the cowl moves with the wedge. In both scenarios one must assume that the incoming fuel and oxidizer are completely mixed; in actuality this is more appropriate for the ram accelerator than the ODWE.

Analysis of the geometry of Fig. 3 leads in general to a complicated interaction of shocks, rarefactions, and combustion processes as the flow propagates between the projectile and cowl surface. To further simplify, we consider only the limit $\tilde{H} \rightarrow \infty$, Fig. 4. Consequently, our geometry shares only a rudi-

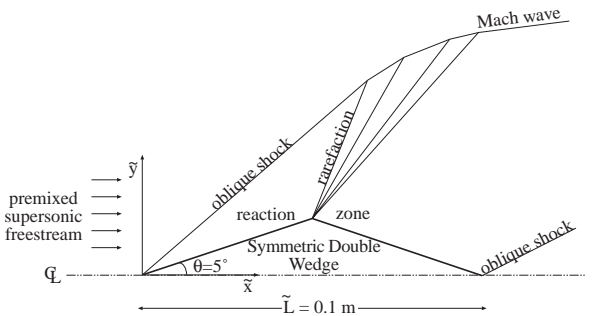


Figure 4: Detailed schematic for $\tilde{H} \rightarrow \infty$

mentary resemblance to actual devices, but has the advantage of being amenable to simple analysis.

Again for tractability, the flow model employed also has only a rudimentary resemblance to commonly used models for real devices. We consider a calorically perfect ideal reacting gas with one-step irreversible Arrhenius kinetics; the reactants and products are taken to have the same molecular weights and material properties. Fig. 4 indicates the general flow features. The ambient, premixed freestream fluid encounters an attached oblique shock at the leading edge of the projectile. No appreciable reaction occurs within the shock or near the front of the projectile. Near the apex of the wedge appreciable reaction begins, and at the apex the flow is turned

through a centered Prandtl-Meyer expansion until it attains a velocity parallel to the lee wedge surface. The reaction then proceeds to completion on the leeward side of the projectile. The flow passes through a final oblique shock at the tail of the projectile, resulting in a velocity only in the \tilde{x} direction. The net force on the projectile is determined by integrating the pressure over the entire surface area.

Model Equations

The model equations are taken to be the unsteady Euler equations and species evolution equation for a reactive calorically perfect ideal gas. These are expressed in dimensionless form below:

$$\frac{d\rho}{dt} + \rho \frac{\partial v_i}{\partial x_i} = 0, \quad (1)$$

$$\frac{dv_i}{dt} + \frac{1}{\rho} \frac{\partial P}{\partial x_i} = 0, \quad (2)$$

$$\frac{dP}{dt} - \gamma \frac{P}{\rho} \frac{d\rho}{dt} = (\gamma - 1) \rho \kappa q (1 - \lambda) \exp\left(\frac{-\Theta}{T}\right), \quad (3)$$

$$\frac{d\lambda}{dt} = \kappa (1 - \lambda) \exp\left(\frac{-\Theta}{T}\right), \quad (4)$$

$$e = \frac{1}{\gamma - 1} \frac{P}{\rho} - \lambda q, \quad (5)$$

$$P = \rho T. \quad (6)$$

The independent variables in Eqs. (1–6) are the density ρ , the Cartesian velocity component v_i , the pressure P , the temperature T , the internal energy e , and the reaction progress variable λ . The dependent variables are time t and the Cartesian position coordinate x_i . The dimensionless parameters are the ratio of specific heats γ , a kinetic parameter κ , the heat of reaction q , and the activation energy Θ . Here the substantial derivative $\frac{d}{dt} = \frac{\partial}{\partial t} + v_i \frac{\partial}{\partial x_i}$.

Equations (1–3) express conservation principles for mass, momenta, and energy, respectively. Equation (4) is a species evolution equation which incorporates an Arrhenius depletion model. Equations (5–6) are caloric and thermal equations of state. A single, first-order, irreversible, exothermic reaction is employed, $A \rightarrow B$. The reaction progress variable λ ranges from zero before reaction to unity at complete reaction. Species mass fractions, Y_i are related to the reaction progress variable by the formulæ, $Y_A = 1 - \lambda$, $Y_B = \lambda$. Initial pre-shock conditions are specified as $\rho = 1$, $u = \sqrt{\gamma} M_0$, $v = 0$, $P = 1$, $T = 1$, $e = 1/(\gamma - 1)$, and $\lambda = 0$. Here M_0 is the freestream Mach number.

In Eqs. (1-6) pressure, density, and temperature are scaled so their pre-shock values are unity; velocities are scaled by a number closely related to the pre-shock acoustic speed. The length of the projectile \tilde{L} is chosen as the reference length scale. The reference time is closely related to the time for a fluid particle to traverse the length of the projectile. In terms of dimensional (indicated by the notation “~”) variables, parameters, and pre-shock ambient conditions (indicated by the subscript “0”), the dimensionless variables are defined by

$$\begin{aligned} \rho &= \frac{\tilde{\rho}}{\tilde{\rho}_0}, & P &= \frac{\tilde{P}}{\tilde{P}_0}, & T &= \frac{\tilde{R}}{\tilde{P}_0/\tilde{\rho}_0} \tilde{T}, \\ u &= \frac{\tilde{u}}{\sqrt{\tilde{P}_0/\tilde{\rho}_0}}, & v &= \frac{\tilde{v}}{\sqrt{\tilde{P}_0/\tilde{\rho}_0}}, & e &= \frac{\tilde{e}}{\tilde{P}_0/\tilde{\rho}_0}, \\ x &= \frac{\tilde{x}}{\tilde{L}}, & y &= \frac{\tilde{y}}{\tilde{L}}, & t &= \frac{\sqrt{\tilde{P}_0/\tilde{\rho}_0}}{\tilde{L}} \tilde{t}. \end{aligned} \quad (7)$$

The dimensionless parameters are defined by the following relations:

$$\begin{aligned} q &= \frac{\tilde{q}}{\tilde{P}_0/\tilde{\rho}_0}, & \Theta &= \frac{\tilde{E}}{\tilde{P}_0/\tilde{\rho}_0}, & \gamma &= 1 + \frac{\tilde{R}}{\tilde{c}_v}, \\ \kappa &= \frac{\tilde{L}}{\sqrt{\tilde{P}_0/\tilde{\rho}_0}} \tilde{k}, & M_0 &= \frac{\tilde{u}_0}{\sqrt{\gamma \tilde{P}_0/\tilde{\rho}_0}}. \end{aligned} \quad (8)$$

Here the dimensional parameters are \tilde{q} the heat of reaction, \tilde{E} the activation energy, \tilde{R} the gas constant for the particular fluid, \tilde{c}_v the specific heat at constant volume, and \tilde{k} the kinetic rate constant.

Numerical Analysis

A numerical analysis of Eqs. (1–6) was performed using a new code²¹ based on the Roe method. In brief, the code uses an explicit Roe scheme⁵ and fractional stepping to integrate the equations in a generalized, curvilinear coordinate system. The integration has second-order spatial accuracy and first-order temporal accuracy. In the implementation of the Roe scheme, all eigenvalues and eigenvectors of the generalized flux Jacobian matrices were obtained analytically, resulting in an efficient yet robust code. The second-order spatial accuracy was obtained using a modified version of the higher-order TVD schemes for Roe averaging suggested by Chakravarthy and Osher²².

The code works in a finite volume sense, requiring flux boundary conditions on all sides of the domain. At the inflow, all fluxes were specified based upon

the chosen inflow quantities. At the projectile surface, slip wall boundary fluxes were specified by setting the transverse component of the velocity (in the curvilinear space) to zero. The only nonzero components of the transverse flux then involved the pressure at the projectile surface. This was estimated by using one-dimensional Riemann invariants and the nearest cell centered quantities, as suggested by Dadone and Grossman²³. Lastly, the nonreflective boundary conditions suggested by Thompson²⁴ were specified at the outflow. This method utilizes the characteristic formulation of the equations to remove reflections from the outflow boundary. Basically, outflowing characteristics are calculated with upwind differencing, while any inflowing characteristics are set to zero. The boundary at the top of the computational domain was treated as a wall, but this had no effect on the solutions presented here since in all cases the oblique shock/detonation exited through the rear boundary without touching the top of the domain. Thus, this was essentially a freestream condition.

Two one-dimensional test cases were used to verify the method. First, the classical Riemann problem was considered (see *e.g.* Hirsch²⁵, pp. 204–211). Figure 5 indicates the solutions obtained at $\tilde{t} = 0.0039$ s for initial pressure and density ratios of 100. Here all quantities have been nondimensionalized by their peak values. The numerical method does an excel-

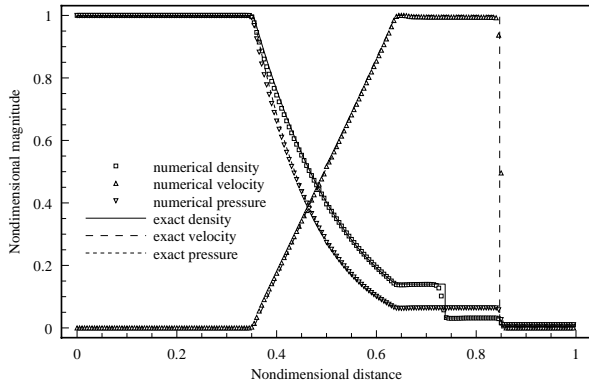


Figure 5: Comparison of exact and numerical Riemann problem solutions.

lent job of matching the exact solution. The weakest agreement is near the contact discontinuity, which is apparent in the first “step” of the density curve. Shock discontinuities, evident in all the variables, are captured very well in only a few points.

A more stringent test of the method was considered next. It is well known that for certain values of q , Θ , and overdrive f , one-dimensional detonation solutions of Eqs. (1-6), known as

Zeldovich-von Neumann-Doering (ZND) detonations, are unstable^{26,27}. Overdrive is defined as $f = (D/D_{CJ})^2$, where D is the speed of the piston supported travelling detonation, D_{CJ} is the speed of an unsupported, freely travelling detonation, and CJ denotes the Chapman-Jouguet condition. Fickett and Wood²⁸, and more recently Bourlioux, Majda, and Roytburd²⁹, have calculated the behavior of these unstable detonations. Since the linear stability limits of the detonation are well known, a severe test of a method is to see if it correctly predicts steady and unsteady detonations near stability boundaries. In each of the cases presented below, the initial conditions for the computations were the exact, steady ZND detonation. The legends of each graph indicate the total number of points used in the computational domain, as well as the number of points contained in the half reaction zone length ($\tilde{L}_{1/2}$) of the initial ZND solution. The half reaction zone length is defined as the distance between the detonation front and the point at which the reaction is halfway to completion. Also, for ease of comparison, the nondimensional time shown is that of Ref. 28, in which the nondimensionalizing parameter is the time ($\tilde{t}_{1/2}$) for a fluid particle to cross the half reaction zone length.

Figure 6 indicates peak detonation pressure versus time for a detonation on the unstable side of the stability boundary. The numerical solution predicts an

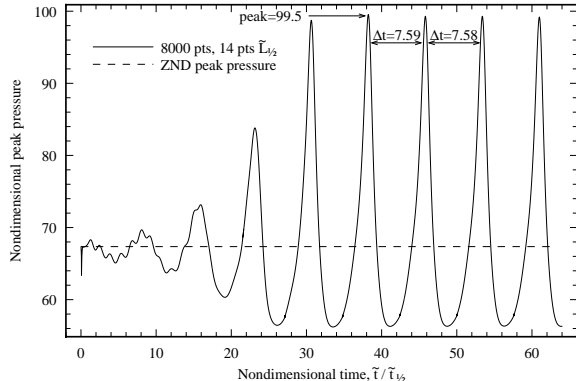


Figure 6: Unsteady ZND detonation ($f = 1.6$, $\Theta = 50$, $q = 50$, $\gamma = 1.2$).

oscillating peak pressure whose amplitude and period agree well with previous numerical solutions²⁹. Figure 7 indicates the results for a detonation on the stable side of the stability boundary. The numerical solution shows some initial oscillation, but this quickly dampens and correctly approaches a steady value very close to the ZND peak pressure. Using more points in the computational domain resulted in the numerical solution more closely approaching

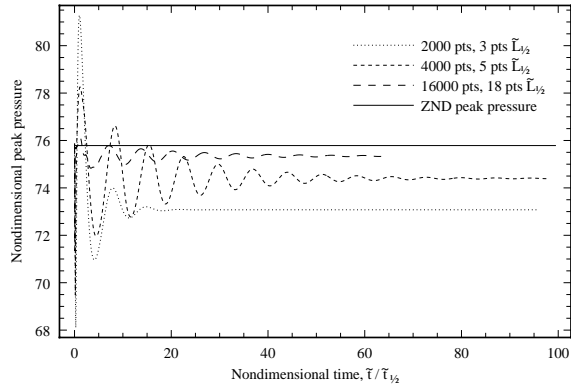


Figure 7: Steady ZND detonation ($f = 1.8$, $\Theta = 50$, $q = 50$, $\gamma = 1.2$).

the ZND pressure. A number of cases even closer to the stability boundaries were examined, and in each one the method correctly predicted the steady or unsteady behavior.

Results

Steady propagation speeds were sought which gave rise to a force balance as the heat release parameter q was varied, $11.908 \leq q \leq 13.456$. Other parameters were held constant at $\gamma = 7/5$, $\theta = 5^\circ$, $\Theta = 12.32$, and $\kappa = 9,179$. For presentation of results the corresponding dimensional values were $\tilde{P}_0 = 1.01325 \times 10^5 \text{ Pa}$, $\tilde{\rho}_0 = 1.225 \text{ kg/m}^3$, $\tilde{k} = 2.64 \times 10^7 \text{ s}^{-1}$, $\tilde{E} = 1.019 \times 10^6 \text{ J/kg}$, $\tilde{L} = 0.1 \text{ m}$, $\tilde{R} = 287 \text{ J/(kgK)}$, $\tilde{c}_v = 717.5 \text{ J/(kgK)}$, $0.985 \times 10^6 \text{ J/kg} \leq \tilde{q} \leq 1.113 \times 10^6 \text{ J/kg}$. These values were chosen not so much to model a real system but so that the method could be successfully illustrated and an interesting bifurcation phenomenon predicted. For models which better represent physical systems, it is certain that the method given here can be applied and plausible that the predictions will have the same essence. A common 199×99 fixed computational grid was used in all cases. Convergence to steady-state was typically achieved in about 5000 time iterations, requiring about three hours of computing time on an IBM RS/6000 POWERstation 350 having 64 Mb RAM and rated at 18.6 MFlops.

The Chapman-Jouguet Mach number (M_{0CJ}) is determined solely by q and γ ²⁶; for the parameters listed $4.275 \leq M_{0CJ} \leq 4.517$. For cases attempted in which $M_0 \leq M_{0CJ}$, a normal detonation would form and propagate forward in the domain until it hit the inflow boundary. This corresponds to the detonation attempting to reach its natural, unsupported propagation speed. Therefore, all cases considered here

were well above M_{0CJ} ; the range of inflow Mach number was $5.5 \leq M_0 \leq 8.5$.

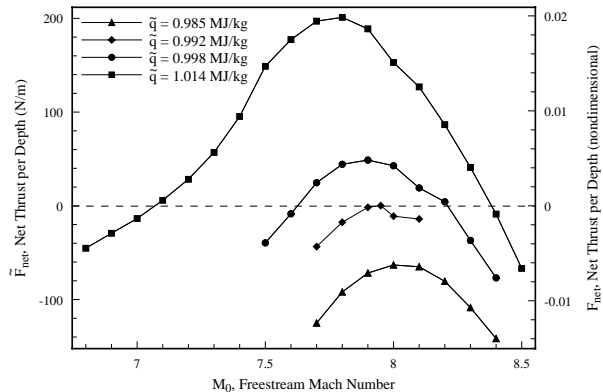


Figure 8: Net thrust force versus Mach number for varying heat release.

The projectile achieves a steady velocity when the force due to pressure wave drag, which tends to retard the motion, is balanced by forces induced by combustion, which tend to accelerate the projectile. The dimensionless net force per unit depth F_{net} is given by the pressure force integrated over the circumference of the diamond-shaped wedge:

$$F_{net} = \oint P n_i ds, \quad (9)$$

where ds is an element of arc length of the diamond-shaped wedge of Fig. 3. Due to symmetry, the only non-zero component of F_{net} is in the x direction. This force is defined to be positive if it points in the negative x direction. For the numerical analysis, numerical integration of the pressure field gave the net thrust. Figure 8 shows F_{net} is plotted vs. M_0 for the three indicated values of \tilde{q} .

For low heat release F_{net} is negative; the thrust force induced by combustion is not sufficient to overcome the wave drag. At a critical value of heat release, $\tilde{q} = 0.992 \text{ MJ/kg}$ ($q = 11.993$), there is a balance of combustion-induced thrust and drag such that $F_{net} = 0$. This occurs at $M_0 = 7.95$. As heat release continues to increase, there are two distinct Mach numbers for which there is no net thrust. A perturbation in the Mach number for the steady solution at the lower Mach number results in a net force which tends to accelerate the projectile away from the equilibrium Mach number. Consequently, this is a statically unstable equilibrium. In the same manner, the equilibrium solution at the higher Mach number is statically stable to such perturbations. As heat release is increased, the stable equilibrium Mach number increases and the reaction zone is located closer

to the expansion fan, while the unstable Mach number decreases and the reaction zone is located closer to the trailing edge. The same trends of these numerical results can be predicted with a simple Rankine-Hugoniot analysis combined with thermal explosion theory^{3,4}.

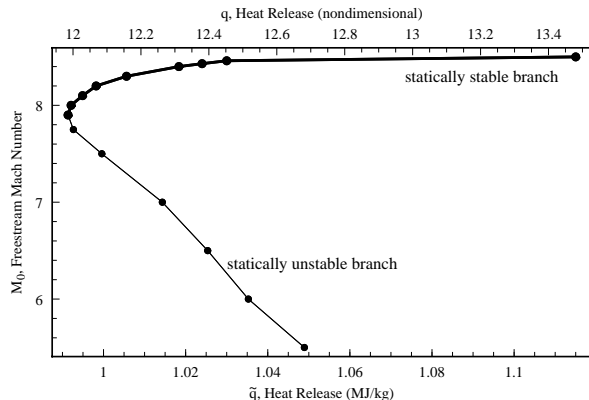


Figure 9: Bifurcation diagram for steady state speed versus heat of reaction.

These results are summarized in the bifurcation diagram shown in Fig. 9, where equilibrium Mach numbers M_0 versus heat release \tilde{q} are plotted. The lower branch is unstable while the upper branch is stable. On the stable branch near the bifurcation point, an increase in \tilde{q} causes the flight speed to increase. The solutions shown here correspond to stable flight speeds in the range of $2,700 \text{ m/s} \lesssim \tilde{u}_0 \lesssim 2,900 \text{ m/s}$, $7.9 \lesssim M_0 \lesssim 8.5$.

For a particular value of heat release, $\tilde{q} = 1.014 \text{ MJ/kg}$, detailed plots of pressure contours and product mass fraction (λ) contours are given for the stable case ($M_0 = 8.4$) and the unstable case ($M_0 = 7.1$) in Figs. 10, 11, 12, 13, respectively. In the stable configuration, the lead oblique shock undergoes a sudden increase in angle of inclination from approximately 11° to 31° . A similar rise from 12° to 38° occurs for the unstable case. This appears to be associated with the chemical reaction. The reaction occurs sooner for the stable case which is at the higher Mach number. This is readily apparent in the product mass fraction contours. Along the wedge surface chemical reaction reaches completion very near the apex for the stable case, while in the unstable case the reaction completes further downstream. This may be explained in the following way: for low M_0 , chemical reaction occurs off the leeward wedge surface far downstream, resulting in a net drag force. As the Mach number is increased, the reaction moves forward onto the wedge, eventually reaching a point at which the wave

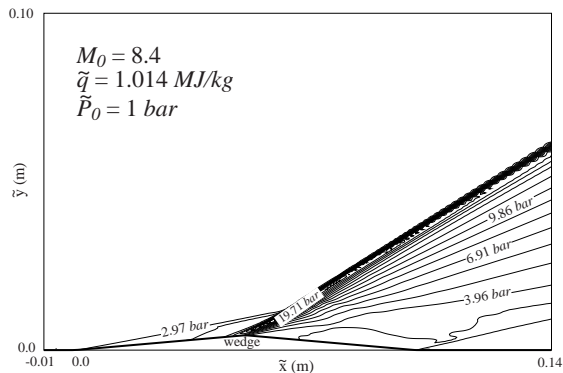


Figure 10: Pressure contours for statically stable steady configuration.

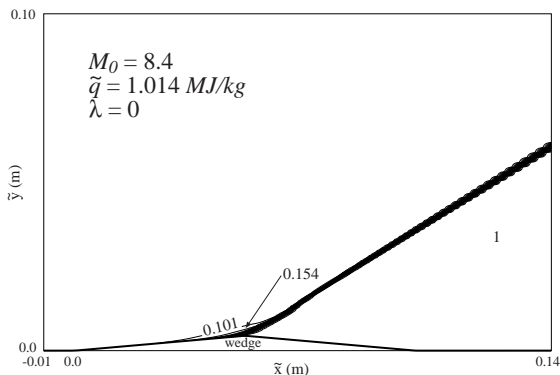


Figure 11: Product mass fraction contours for statically stable configuration.

drag of the projectile is balanced by the thrust due to chemical reaction. Increasing M_0 past this equilibrium point moves the reaction closer to the wedge apex on the leeward side, resulting in positive F_{net} . Increasing M_0 still further pushes the reaction over the apex and onto the front of the wedge. The pressure increase due to chemical reaction on the front of the wedge is then balanced by the resulting higher pressure on the leeward side of the wedge.

Figure 14 shows plots of the pressures along the lines of symmetry and projectile surface for the stable and unstable cases of interest. Here there are about 90 grid points distributed on the wedge surface. As a verification of the code's ability to predict two-dimensional flows, plots of the exact and numerical pressure traces for an inert flow over the projectile are also given. The numerical pressure closely follows the exact solution, showing the biggest dis-

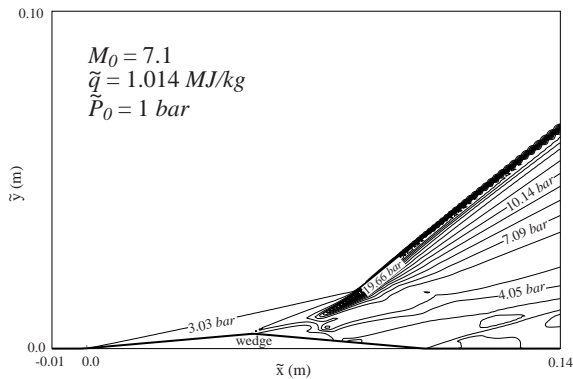


Figure 12: Pressure contours for statically unstable steady configuration.

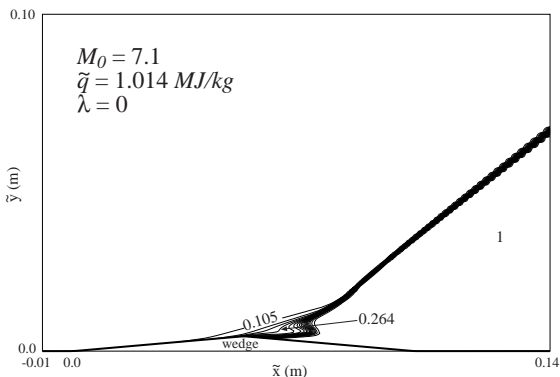


Figure 13: Product mass fraction contours for statically unstable steady configuration.

crepancies at the shock and rarefaction discontinuities. The discontinuities are still captured well, however, and there is no evidence of any Gibbs phenomena. Between the discontinuities the numerical solution reaches constant states very close to those of the exact solution. Drag calculations for the exact and numerical solutions show that they are in excellent agreement.

Considering the surface pressure for the stable case in Fig. 14, it is apparent that significant reaction occurs on the front face of the wedge. The pressure begins to rise slowly following the initial shock, and then very suddenly prior to the rarefaction at the wedge apex. Following the apex the pressure remains well above the inert case, and then jumps again because of the trailing shock at the end of the projectile. The unstable case shows a much different solution. Once again the pressure begins to rise slowly following the

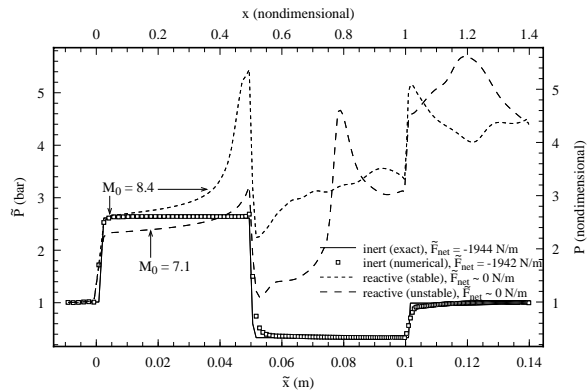


Figure 14: Pressure traces on wedge surface.

initial shock, but in this case the peak prior to the rarefaction is much lower. The pressure drops through the rarefaction discontinuity, but once again remains above the inert pressure. The pressure peaks on the back of the wedge where the reaction reaches completion, and then jumps through the trailing shock. This is consistent with the prior discussion.

Finally, it is noted that in the far-field limit, the oblique shock should relax to a Mach wave with insufficient strength to ignite the mixture. Apparently the domain is not sufficiently large to capture this, though it should not affect the pressure distribution on the wedge surface.

Conclusions

This study has given indication of the importance of the interaction of kinetic length scales with geometric length scales in determining steady propagation velocities for high Mach number propulsion devices. The trends of our variation of net thrust with Mach number for fixed heat release are consistent with those of Refs. 1 and 2. Most importantly, the idea of using the heat release to vary the propagation speed, as shown in the bifurcation diagrams, has been demonstrated. In an ODWE environment, the equivalence ratio could presumably be varied to achieve this effect. Alternatively, one may be able to use the wedge angle as a bifurcation parameter to vary the propagation speed.

In the results presented here the oblique detonations exhibited no instabilities. Since the code is time accurate and the numerical method capable of capturing such instabilities, this would seem to suggest that the oblique detonations were stable. However, there were as few as 3-4 cells within the reaction zones of the detonations. The one-dimensional ZND results indicate that this is too few to accurately capture the possible unsteady behavior of the detonation, though

unsteady solutions were still found with very few cells in the reaction zone. More refined numerical solutions and comparisons to one-dimensional instability are required to completely assess oblique detonation stability.

For the future it would be useful to consider the case of dynamic stability. This would be accomplished by considering the equations of motion in an accelerating frame of reference. The computed forces on the projectile would enter into the acceleration of the reference frame, which would then alter the inflow Mach number dynamically. Also as suggested in an upcoming review by Powers³⁰, it would be useful to study this problem in the context of other well-documented inert flows such as a Busemann biplane or flow over a thin airfoil.

Acknowledgments

The study has received partial support from the Indiana Space Grant Consortium sponsored by NASA Headquarters. The authors acknowledge the contributions of Mr. John R. Roof IV, who with the support of the NASA-sponsored Research Experience for Undergraduates program, assisted with many numerical calculations.

References

- ¹Brackett, D. C., and Bogdanoff, D. W., "Computational Investigation of Oblique Detonation Ramjet-in-Tube Concepts," *Journal of Propulsion and Power*, Vol. 5, No. 3, 1989, pp. 276–281.
- ²Yungster, S., and Bruckner, A. P., "Computational Studies of a Superdetonative Ram Accelerator Mode," *Journal of Propulsion and Power*, Vol. 8, No. 2, 1992, pp. 457–463.
- ³Powers, J. M., and Gonthier, K. A., "Methodology and Analysis for Determination of Propagation Speed of High-Speed Propulsion Devices," Proceedings of the Central States Section Spring 1992 Technical Meeting of the Combustion Institute, April 1992, pp. 1–6.
- ⁴Powers, J. M., Fulton, D. R., Gonthier, K. A., and Grismer, M. J., "Analysis for Steady Propagation of a Generic Ram Accelerator/Oblique Detonation Wave Engine," AIAA Paper 93-0243, January 1993.
- ⁵Roe, P. L., "Approximate Riemann Solvers, Parameter Vectors, and Difference Schemes," *Journal of Computational Physics*, Vol. 43, 1981, pp. 357–372.
- ⁶Hertzberg, A., Bruckner, A. P., and Bogdanoff, D. W., "Ram Accelerator: A New Chemical Method for Accelerating Projectiles to Ultrahigh Velocities," *AIAA Journal*, Vol. 26, No. 2, 1988, pp. 195–203.
- ⁷Hertzberg, A., Bruckner, A. P., and Knowlan, C., "Experimental Investigation of Ram Accelerator Propulsion Modes," *Shock Waves*, Vol. 1, 1991, pp. 17–25.
- ⁸Yungster, S., Eberhardt, S., and Bruckner, A. P., "Numerical Simulation of Hypervelocity Projectiles in Detonable Gases," *AIAA Journal*, Vol. 29, No. 2, 1991, pp. 187–199.
- ⁹Yungster, S., "Numerical Study of Shock-Wave/Boundary-Layer Interactions in Premixed Combustible Gases," *AIAA Journal*, Vol. 30, No. 10, 1992, pp. 2379–2387.
- ¹⁰Dunlap, R., Brehm, R. L., and Nicholls, J. A., "A Preliminary Study of the Application of Steady-State Detonative Combustion to a Reaction Engine," *Jet Propulsion*, Vol. 28, No. 7, 1958, pp. 451–456.
- ¹¹Cambier, J. L., Adelman, H., and Menees, G. P., "Numerical Simulations of Oblique Detonations in Supersonic Combustion Chambers," *Journal of Propulsion and Power*, Vol. 5, No. 4, 1989, pp. 483–491.
- ¹²Cambier, J. L., Adelman, H., and Menees, G. P., "Numerical Simulations of an Oblique Detonation Wave Engine," *Journal of Propulsion and Power*, Vol. 6, No. 3, 1990, pp. 315–323.
- ¹³Bruckner, A. P., Knowlan, C., Hertzberg, A., and Bogdanoff, D. W., "Operational Characteristics of the Thermally Choked Ram Accelerator," *Journal of Propulsion and Power*, Vol. 7, No. 5, 1991, pp. 828–836.
- ¹⁴Pratt, D. T., Humphrey, J. W., and Glenn, D. E., "Morphology of Standing Oblique Detonation Waves," *Journal of Propulsion and Power*, Vol. 7, No. 5, 1991, pp. 837–845.
- ¹⁵Bogdanoff, D. W., "Ram Accelerator Direct Space Launch System: New Concepts," *Journal of Propulsion and Power*, Vol. 8, No. 2, 1992, pp. 481–490.
- ¹⁶Powers, J. M., and Stewart, D. S., "Approximate Solutions for Oblique Detonations in the Hypersonic Limit," *AIAA Journal*, Vol. 30, No. 3, 1992, pp. 726–736.
- ¹⁷Powers, J. M., and Gonthier, K. A., "Reaction Zone Structure for Strong, Weak Overdriven, and Weak Underdriven Oblique Detonations," *Physics of Fluids A*, Vol. 4, No. 9, 1992, pp. 2082–2089.
- ¹⁸Grismer, M. J., and Powers, J. M., "Comparisons of Numerical Oblique Detonation Solutions with an Asymptotic Benchmark," *AIAA Journal*, Vol. 30, No. 12, 1992, pp. 2985–2987.
- ¹⁹Pepper, D. W., and Brueckner, F. P., "Simulation of an Oblique Detonation Wave Scramjet Accelerator for Hypervelocity Launchers," in *Computers and Computing in Heat Transfer Science and Engineer-*

ing, W. Nakayama and K. T. Yang, eds., CRC Press, Boca Raton, Florida, 1993, pp. 119–137.

²⁰Wilson, G. J., and Sussman, M. A., “Computation of Unsteady Shock-Induced Combustion Using Logarithmic Species Conservation Equations,” *AIAA Journal*, Vol. 31, No. 2, 1993, pp. 294–301.

²¹Grismer, M. J., “Unsteady Oblique Detonations”, Ph.D. Thesis in preparation, University of Notre Dame.

²²Chakravarthy, S. R. and Osher, S., “A New Class of High Accuracy TVD Schemes for Hyperbolic Conservation Laws,” AIAA 85-0363, January 1985.

²³Dadone, A. and Grossman, B., “Characteristic-Based, Rotated Upwind Scheme for the Euler Equations,” *AIAA Journal*, Vol. 30, No. 9, 1992, pp. 2219–2226.

²⁴Thompson, K. W., “Time Dependent Boundary Conditions for Hyperbolic Systems,” *Journal of Computational Physics*, Vol. 68, 1987, pp. 1–24.

²⁵Hirsch, C., *Numerical Computation of Internal and External Flows, Volume 2: Computational Methods for Inviscid and Viscous Flows*, John Wiley & Sons, New York, 1990.

²⁶Fickett, W. and Davis, W. C., *Detonation*, University of California Press, Berkeley, 1979.

²⁷Lee, H. I., and Stewart, D. S., “Calculation of Linear Detonation Instability: One-Dimensional Instability of Plane Detonation,” *Journal of Fluid Mechanics*, Vol. 216, 1990, pp. 103–132.

²⁸Fickett, W. and Wood, W. W., “Flow Calculations for Pulsating One-Dimensional Detonations,” *The Physics of Fluids*, Vol. 9, No. 5, 1966, pp. 903–916.

²⁹Bourlioux, A., Majda, A. J., and Roytburd, V., “Theoretical and Numerical Structure for Unstable One-Dimensional Detonations,” *SIAM Journal of Applied Mathematics*, Vol. 51, No. 2, 1991, pp. 303–343.

³⁰Powers, J. M., “Oblique Detonations: Theory and Propulsion Applications,” to appear in *Combustion in High-Speed Flows*, J. Buckmaster, T. L. Jackson, and A. Kumar, eds., Kluwer Academic Publishers, 1994.